Journal of Marine Science and Technology, Vol. 28, No. 6 pp. 528-537 (2020)
DOI: 10.6119/JMST.202012_28(6).0008

STUDY ON UNDERWATER NAVIGATION FOR AN UNDERWATER TRACK VEHICLE

Dae-Hyeong Ji[1], Hyeung-Sik Choi[2], Sang-Ki Jeong[3], Hyun-Joon Cho[2], Ji-Hyeong Lee[2], and Wen-Hsiang Hsieh[4]

Key words: underwater navigation, underwater track vehicle, inertial navigation system, dead reckoning, ultra-short baseline.

ABSTRACT

In this study, an underwater navigation algorithm was developed to apply a navigation system to an underwater track vehicle (UTV). Generally, a Doppler velocity log (DVL) is used to obtain the velocity information of underwater vehicles. However, a DVL cannot be used in a UTV owing to vehicle vibration and limited sensing distance. Hence, dead reckoning navigation is typically used, which results in severe errors in altitude and position values over long periods of operation. To address these problems, in this study, we developed a new underwater navigation system for a UTV using navigation sensors comprising an inertial navigation system, an ultra-short baseline, and an encoder sensor on a track wheel. We performed mathematical modeling of the accelerometer, gyroscope, and magnetometer. We constructed a navigation system composed of electronic hardware, a control system, an operating system, and a navigation system and then performed a navigation experiment. Finally, we verified the performance of the developed underwater navigation system using real sea area experiments.

I. INTRODUCTION

An underwater construction robot, a type of track-based remotely operated vehicle (ROV), which can also be called an underwater track vehicle (UTV), uses a water jet or a trenching cutter to excavate the underwater land. To operate as per the desired path and position, the UTV should be able to accurately acquire the hull's posture and position information (Lee et al., 2004).

Inertial navigation is one of the most widely used dead reckoning (DR) systems for trajectory tracking and uses an inertial navigation system (INS) (Yunchun and Farrell, 2003). A typical INS consolidates the measurements from both accelerometers and gyroscopes to continuously estimate the position and orientation of the hull. As various sensor errors are consolidated over time, the INS can only provide accurate and high-frequency (typically in the range of 100 to 200 Hz) information for a short period of time. As a result, errors are particularly high when inexpensive sensors are used. Meanwhile, a global positioning system (GPS) provides globally referenced position and velocity estimates at a low frequency (typically in the range of 1 to 4 Hz). The integration of INS and GPS (INS-GPS) can become a navigation system that utilizes the advantages of both systems and compensates for the disadvantages of the individual systems. Therefore, the integrated INS-GPS system can estimate the overall condition of the vehicle at high frequencies without drift. For a long time, various state estimation techniques have been used to integrate INS and GPS. Sukkarieh et al. (1998), as well as Qi and Moore (2002) proposed a technique that is based on a linear Kalman filtering technique. The Kalman filter (KF), which is commonly used to estimate system state variables and suppress measurement noise, is recognized as one of the most powerful state estimation techniques. Information from other sensors can be structurally merged using a KF.

Owing to its nonlinear characteristics, the extended KF, which is a nonlinear version, is widely used to calculate INS-GPS integration. Ridao et al. (2011) and Ribas et al. (2012) studied the integration of a Doppler velocity log (DVL) which considers the time delay of an ultra-short baseline (USBL) ultrasonic positioning system measurement signal and applied the results to underwater navigation of autonomous underwater vehicles (AUVs). Lee et al. (2007) proposed a complex navigation algorithm that integrated distance information into the inertial navigation algorithm and studied the integration of an USBL, a DVL and an inertial measurement unit (IMU)

Paper submitted 06/01/20; revised 11/18/20; accepted 12/05/20. Corresponding Author: Hyeung-Sik Choi (e-mail: hchoi@kmou.ac.kr)
[1] Marine Security and Safety Research Center, Korea Institute of Ocean Science & Technology, Busan, Korea.
[2] Department of Mechanical Engineering, Korea Maritime and Ocean University, Busan, Korea.
[3] Maritime ICT R&D Center, Korea Institute of Ocean Science & Technology, Busan, Korea.
[4] Department of Automation Engineering, National Formosa University, Yunlin County, 632, Taiwan, ROC.

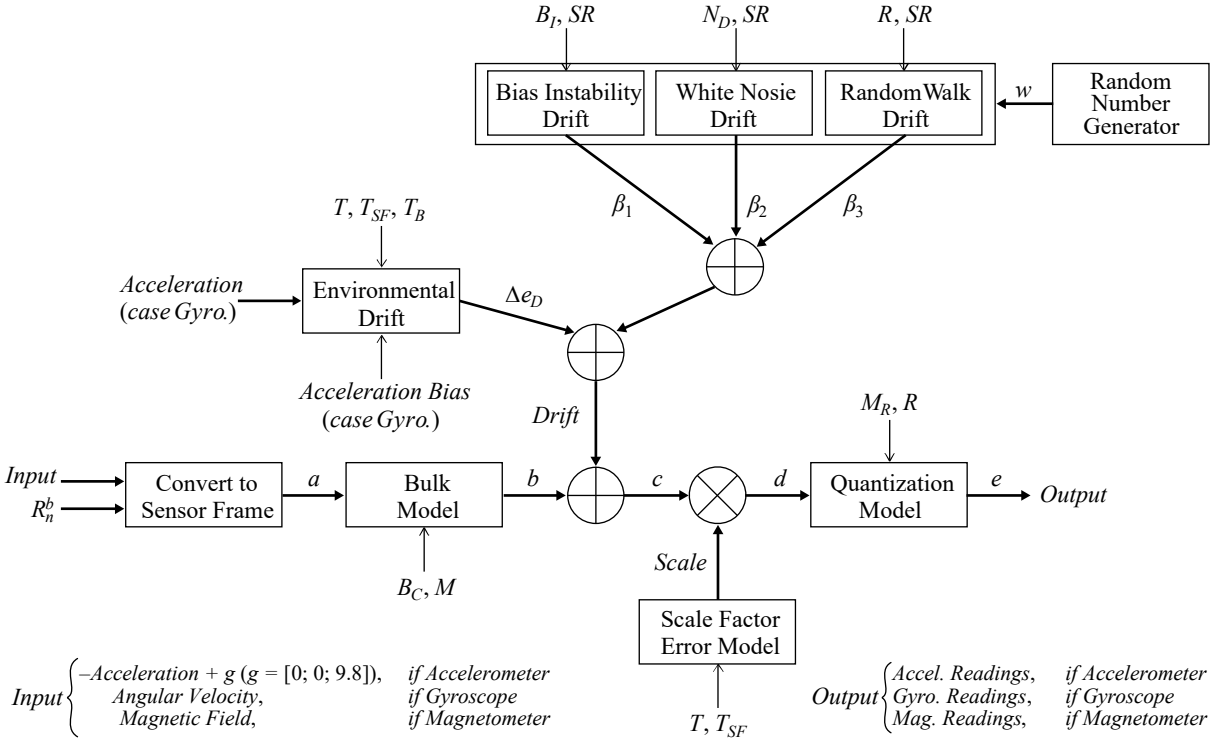

Fig. 1. Block diagram of IMU sensor.

(Jeong et al., 2017; Lee et al., 2017). Jung et al. (2018) proposed an ROV system using an USBL and an IMU. Ji et al. (2019a) proposed an attitude reference system (ARS) using a ring laser gyroscope (RLG).

In general, the sensors used in underwater navigation are IMU, GPS, DVL, USBL and depth sensors (Alahyari et al., 2011). The USBL is an underwater acoustic sensor that measures absolute coordinates in water, which is similar to GPS on land (Penas, 2009). The track robot in this study causes ambient turbidity, thus causing sensor errors from the acceleration signal due to the digging impact. In particular, the DVL, a typical sensor that measures travel speed, cannot be used because of ambient turbidity (Somers, 2011). Therefore, it is necessary to study methods to reduce position error by applying underwater navigation that uses an INS and a USBL other than a DVL.

Classic dead reckoning without a DVL leads to serious errors in altitude and position values (Ji et al., 2019b). Therefore, this study intends to correct the speed by using the information of an encoder on track wheel that can measure a track speed by removing the DVL from the underwater navigation system with INS and USBL.

In this study, we attempt to improve the completeness of designing a navigation algorithm by analyzing the readings recorded from the mathematical models of the accelerometer, angular velocity meter, and magnetometer as well as the parameters of each sensor. In addition, before the navigation system was mounted on the underwater track robot for actual sea performance evaluation, the estimated values for specific missions and unexpected situations were analyzed through computer simulations and the effectiveness of the applied navigation algorithm was verified.

Finally, the performance of the developed underwater navigation system is verified in inland and underwater environments by applying it to an underwater track robot which is the target platform of this study.

II. MATHEMATICAL MODEL OF THE NAVIGATION SENSOR

The IMU is the main sensor in a system that integrates the INS and GPS for position correction. The selection of an IMU is a critical factor that determines the overall performance of an integrated system. It is possible to analyze the error characteristics of the navigation solution by analyzing the characteristics of the errors generated in the IMU. The sensor was modeled using mathematical models of the accelerometer, angular velocity meter, and magnetometer in the IMU as well as the parameters of each sensor.

The mathematical model of an IMU models sensor readings by using directions, physical value inputs, and sensor parameters (Titterton and Weston, 2004; Brunner et al., 2015; Hostettler and Sarkka, 2016; MathWorks, 2018). Fig. 1 shows a block diagram of the model derivation method. The accelerometer, angular velocity meter, and magnetometer are shown in the form of similar block diagrams and the input information is changed for each sensor.

Equation (1) uses a sensor value for the ground to switch

from the local frame to the sensor frame.

$$a = R_n^b \left(\text{input}\right)^T, \text{input} = \begin{cases} \text{if} & accel. = f^n \\ else\,if & gyro. = \omega^n \\ else & mag. = m^n \end{cases} \quad (1)$$

Here, R_n^b is the direction of the IMU, f^n is the acceleration, ω^n is the angular velocity, and m^n is the magnetic vector in the local navigation coordinate system. If the direction is entered in the quaternion format, it is converted into a rotation matrix before processing.

The a for the ground in the sensor frame shown in Equation (2) passes through the bulk model and adds axis misalignment and bias.

$$b = \left(\begin{bmatrix} 1 & \frac{M_2}{100} & \frac{M_3}{100} \\ \frac{M_1}{100} & 1 & \frac{M_3}{100} \\ \frac{M_1}{100} & \frac{M_2}{100} & 1 \end{bmatrix} \left(a^T\right) \right)^T + B_C \quad (2)$$

Here, B_C is a constant sensor offset bias and M is the misalignment of the sensor axes. These are entered as the first, second, and third elements, respectively.

The bias instability drift is modeled as white noise bias before filtering as shown in Equation (3).

$$\beta_1 = h_1 * (w)\left(B_I\right) \quad (3)$$

Here, B_I is the bias offset instability of a sensor, w is a random number given by an attribute, and h_1 is a filter defined by the sample rate (SR) as expressed in Equation (4).

$$H_1(z) = \frac{1}{1 + \left(\frac{2}{SR} - 1\right) z^{-1}} \quad (4)$$

The white noise drift is modeled by multiplying the standard deviation by the random white noise as shown in Equation (5).

$$\beta_2 = (w)\left(\frac{\sqrt{SR}}{2}\right)\left(N_D\right) \quad (5)$$

Here, N_D is the power spectrum (noise density) of a sensor.

The random walk drift is modeled through filtering by biasing the random white noise as shown in Equation (6).

$$\beta_3 = h_2 * (w)\left(\frac{R}{\frac{\sqrt{SR}}{2}}\right) \quad (6)$$

Here, R is the consolidated white noise (random walk) of a sensor, and h_2 is a filter expressed in Equation (7).

$$H_2(z) = \frac{1}{1 + z^{-1}} \quad (7)$$

The environmental drift noise is modeled by multiplying the temperature bias by the difference between the standard and operating temperatures of the sensor, as expressed in Equation (8).

$$\Delta e_D = (T - 25)\left(T_B\right) \quad (8)$$

Here, T is the operating temperature of the sensor, T_B is the temperature bias of the sensor, and the constant 25 is the standard temperature (in °C).

The scale factor error due to temperature was modeled, as expressed in Equation (9).

$$E_{SF} = 1 + \left(\frac{T - 25}{100}\right)\left(T_{SF}\right) \quad (9)$$

Here, E_{SF} is the scale factor error, T_{SF} is the scale factor due to temperature, and the constant 25 is the standard temperature (in °C). In this study, T, the temperature, was 25 °C.

The quantization is modeled by saturating the continuous signal model, as expressed in Equation (10).

$$e = \begin{cases} M_R & \text{if } d \succ M_R \\ -M_R & \text{else if } d \prec -M_R \\ d & \text{else} \end{cases} \quad (10)$$

Here, M_R is a maximum reading value (measurement range) of a sensor and RS, the measurement resolution of a sensor, is configured, as expressed in Equation (11).

$$Output = RS\left(\text{round}\left(\frac{e}{RS}\right)\right) \quad (11)$$

Through the modeling described above, the output values (acceleration, angular velocity, and geomagnetic field strength) of the IMU sensor can be obtained.

III. ALGORITHM OF INTEGRATED NAVIGATION

1. Coordinate System

The origin of the north-east-down (NED) system is on the ground and it rotates with the Earth. As shown in Fig. 2, the X-axis is north, the Y-axis is east, and the Z-axis is toward the center of the Earth.

When considering the Earth as elliptical, the angle between the Z-axis and the equatorial plane is not the geocentric latitude λ,

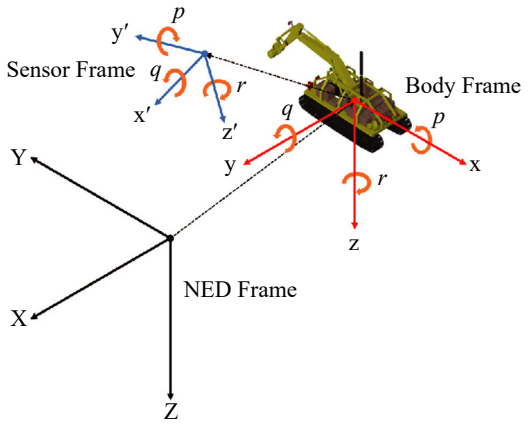

Fig. 2. Coordinate systems.

but the geocentric latitude μ. However, Z can be λ because the Earth model is generally used to analyze the motion characteristics of aircraft assuming the Earth as a complete sphere (Siouris, 2004).

2. Design of Integrated Navigation Algorithm

The system model used an INS error model. An extended KF filter was used to integrate the navigation system. The state variable to be estimated from the KF is given by Equation (12) (Munguia, 2014).

$$X = \left[\delta P_{INS}\ \delta V_{INS}\ \delta\Phi\ \nabla\ \varepsilon\right]^{T} \tag{12}$$

Here, δP_{INS} is the position error vector of the INS, δV_{INS} is the velocity error vector of the INS, $\delta\Phi$ is the distortion error of the INS posture, ∇ is the random bias error of the velocity sensor, and ε is the random bias error of the gyro sensor. The state equation of the KF is shown in Equations (13) and (14) (Park, 2014; Karamat et al., 2015).

$$X(k) = \dot{F}_{INS}(k) + w_{INS} \tag{13}$$

$$F_{INS}(k) = \begin{bmatrix} F_{pp} & F_{pv} & 0_{3\times3} & 0_{3\times3} & 0_{3\times3} \\ F_{vp} & F_{vv} & F_{va} & F_{vb_a} & 0_{3\times3} \\ F_{ap} & F_{av} & F_{aa} & 0_{3\times3} & F_{ab_g} \\ 0_{3\times3} & 0_{3\times3} & 0_{3\times3} & 0_{3\times3} & 0_{3\times3} \\ 0_{3\times3} & 0_{3\times3} & 0_{3\times3} & 0_{3\times3} & 0_{3\times3} \end{bmatrix} \tag{14}$$

Here, the average of the process noise w_{INS} is 0, and the white noise of the angular velocity meter and acceleration meter whose covariance is Q_{INS} can be expressed as in Equation (15).

$$w_{INS} = \left[0_{1\times3}\quad w_{acc}\quad w_{gyro}\quad 0_{1\times6}\right] \tag{15}$$

F_{INS} can be expressed as shown in Equations (16) to (25) from the error model induced above.

$$F_{pv} = \begin{bmatrix} \frac{1}{M+h} & 0 & 0 \\ 0 & \frac{1}{(N+h)\cos\varphi} & 0 \\ 0 & 0 & -1 \end{bmatrix} \tag{16}$$

$$F_{vp} = \begin{bmatrix} 2w_e v_e \cos\varphi - \frac{v_e^2}{(N+h)\cos\varphi}\left(\frac{\sin\varphi}{N+h}N' - \frac{1}{\cos\varphi}\right) + \frac{v_n v_d M'}{M+h} & 0 & \frac{v_n v_d}{(M+h)^2} - \frac{v_e^2 \tan\varphi}{(N+h)^2} \\ 2w_e\left(v_d \sin\varphi - v_n \cos\varphi\right) + \frac{v_n v_e}{(N+h)\cos\varphi}\left(\frac{\sin\varphi}{N+h}N' - \frac{1}{\cos\varphi}\right) + \frac{v_e v_d N'}{(N+h)^2} & 0 & \frac{v_e\left(v_n \tan\varphi + v_d\right)}{(N+h)^2} \\ -\frac{v_n^2}{(M+h)^2} - 2w_e v_e \sin\varphi - \frac{v_e^2 N'}{(N+h)^2} & 0 & \frac{v_e v_d}{(N+h)^2} - v \end{bmatrix} \tag{17}$$

$$F_{pp} = \begin{bmatrix} \frac{-v_n M'}{(M+M'+h)^2} & 0 & \frac{-v_n}{(M+h)^2} \\ \frac{-v_e}{(N+h)^2}\left(\frac{N'}{\cos\varphi} - (N+h)\tan\varphi\right) & 0 & \frac{-v_e}{(N+h)^2\cos\varphi} \\ 0 & 0 & 0 \end{bmatrix} \tag{18}$$

$$F_{ap} = \begin{bmatrix} -w_e \sin\varphi - \frac{v_e N'}{(N+h)^2} & 0 & \frac{-v_e}{N+h} \\ \frac{v_n M'}{M+h} & 0 & \frac{v_n}{(M+h)^2} \\ -w_e \cos\varphi + \frac{v_e}{(N+h)\cos\varphi}\left(\frac{\sin\varphi}{N+h}N' - \frac{1}{\cos\varphi}\right) & 0 & \frac{v_e \tan\varphi}{(N+h)^2} \end{bmatrix} \tag{19}$$

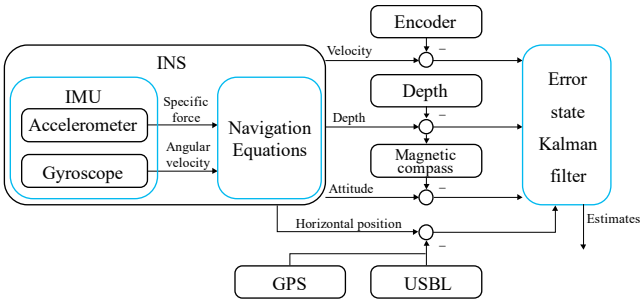

Fig. 3. Block diagram of navigation system.

$$F_{aa}=\begin{bmatrix} 0 & w_e sin\varphi+v_e\frac{tan\varphi}{N+h} & \frac{-v_n}{M+h} \\ -w_e sin\varphi-v_e\frac{tan\varphi}{N+h} & 0 & -w_e cos\varphi+\frac{v_e}{N+h} \\ \frac{v_n}{M+h} & w_e cos\varphi+\frac{v_e}{N+h} & 0 \end{bmatrix} \tag{20}$$

$$F_{vv}=\begin{bmatrix} -\frac{v_d}{M+h} & -\frac{v_e tan\varphi}{N+h} & 0 \\ 0 & \frac{-v_n tan\varphi-v_d}{N+h} & 0 \\ \frac{v_n}{M+h} & \frac{v_e}{N+h} & 0 \end{bmatrix} \tag{21}$$

$$F_{av}=\begin{bmatrix} 0 & \frac{1}{N+h} & 0 \\ -\frac{1}{M+h} & 0 & 0 \\ 0 & -\frac{tan\varphi}{N+h} & 0 \end{bmatrix} \tag{22}$$

$$F_{va}=C_b^n a_b \tag{23}$$

$$F_{vb_a}=C_n^b \tag{24}$$

$$F_{ab_g}=C_b^n \tag{25}$$

In the weakly coupled type, the measurement error of the two navigation systems can be calculated by the difference between the position and velocity information. At this moment, H is a measurement matrix and can be expressed as in Equation (26).

$$z=\begin{bmatrix} P_{INS} \\ V_{INS} \end{bmatrix}-\begin{bmatrix} P_{GPS\|USBL} \\ V_{GPS\|USBL} \end{bmatrix}=HX+v_{INS} \tag{26}$$

$$H=\begin{bmatrix} I_{6\times6} & 0_{6\times9} \end{bmatrix} \tag{27}$$

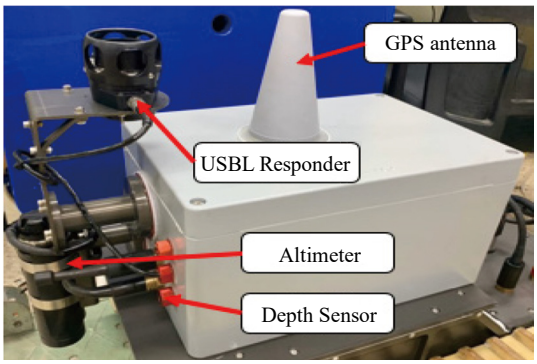

Fig. 4. Developed underwater navigation system

3. Configuration of the Integrated Navigation Algorithm

The integrated navigation algorithm proposed in this study is shown in Fig. 3. As described above, the INS was configured using an IMU. The velocity derived from the INS was corrected with a track encoder, the position was corrected with a GPS or USBL (horizontal), and depth sensor (vertical), and the direction angle was corrected with a magnetometer. If the accuracy of the measured position is low in the USBL position correction step, the weight of the step where the velocity is corrected with encoder information varies. Meanwhile, when the position accuracy of the USBL increases, the weight of the position correction step increases, and the weight of the velocity correction step is variably lowered. Similarly, the weight of the position/velocity correction step varies according to the position accuracy of the USBL. Finally, the resulting value (velocity, position, and direction angle) was derived from the extended KF.

Additionally, the horizontal position drift of the integrated navigation is determined by the error of the estimated Earth's fixed velocity (i.e., north or east velocity). The main reason for this error is the fixed velocity error and heading error of the hull. The high-frequency velocity error is estimated by the IMU, the fixed velocity errors of the hull. Without velocity correction by the encoder, even the most accurate INS can have a large velocity uncertainty after a short period of time. This can remove the weakness of the frequency error of the DVL which is used in a general underwater navigation system.

IV. CONFIGURATION AND PERFORMANCE TEST OF UNDERWATER NAVIGATION SYSTEM AND PLATFORM

1. Underwater Navigation System

A photograph of the underwater navigation system developed in this study is shown in Fig. 4. The exterior of the system uses a waterproof box-shaped aluminum case, which is designed to mount a GPS antenna on the top, an altimeter at the side, and an USBL responder at the side above the altimeter. A small-sized USBL was selected as the sensor for use on a small platform. Inside the system, there are sensors for navigation

Table 1. Specifications of underwater navigation system.

Index	Value	Units
Length	420	mm
Width	300	mm
Height	300	mm
Weight (dry)	8	kg
Weight (water)	2	kg
Standard components	RLG, Depth, USBL, GPS, TCM, Altimeter, Leak sensor, Ethernet Hub	

Table 2. Specifications of underwater track vehicle.

Index	Value	Units
Length	600	mm
Width	500	mm
Height	250	mm
Weight (dry)	35	kg
Weight (water)	10	kg
Standard components	Ethernet Hub, 200W BLDC motor, Motor drive, Battery	

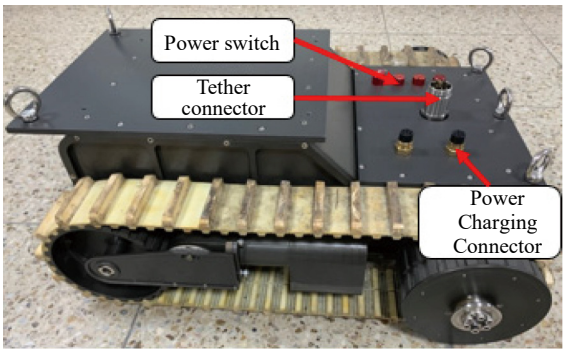

Fig. 5. Developed Underwater track vehicle.

calculation, a leak sensor for leak measurement, an Ethernet hub for communication, and an interface board for power supply and data communication to the sensors. The RLG was selected instead of the MEMS-type IMU to increase the computational performance of the INS. Table 1 lists the specifications and components of the underwater navigation system.

2. Configuration of Underwater Track Robot Platform

The underwater track robot built to test the performance of the developed underwater navigation system is shown in Fig. 5. The figure also shows that the platform has two caterpillars to enable movement on both the land and seafloor. The upper part was designed to be equipped with an underwater navigation system. Table 2 lists the specifications and equipment of the underwater track robot. The platform dimensions were 600 mm long, 500 mm between the endpoints of the caterpillars, and 250 mm from the bottom to the top. A total of two BLDC motors independently control each caterpillar and are designed to allow forward/reverse and left/right turns depending on the control method.

Table 3. Specifications of sensors used in ground experiments.

Index		Value		Units
RLG	Operating Range	Gyro	Acc.	°/sec, g
		1074	70	
	Scale Factor Linearity	150	300	PPM
	Bias Repeatability	1	1	°/hr, m-g
	Bias Stability	1	1	°/hr, m-g
	Update Rate	100		Hz
GPS	Position Accuracy	1.3(H), 1.9(V)		m
	Update Rate	1		Hz
Magnetic compass	Measurement Range	80		μT
	Resolution	0.05		μT
	Repeatability	0.1		μT
	Update Rate	30		Hz
Encoder	Counts per turn	500		-
	Max. speed	24000		Rpm
	Update Rate	10		Hz

3. Test of Integrated Navigation Performance Applied to Underwater Track Robot

The integrated navigation performance was tested on land using the developed underwater navigation system and an underwater track robot. The speed was corrected by applying the encoder information in the integrated final navigation algorithm. The latitude and longitude of the test area were 35°04'25.49″ N and 129°05'17.13″ E, and the GPS was used on land for the same purpose as that of the USBL, which was used for underwater positioning. To increase the GPS reception sensitivity, the experiment was performed on a playground that was not surrounded by tall buildings. The specifications of the sensors used in the experiments are listed in Table 3.

Acceleration and angular velocity information were obtained using an RLG to estimate the angle/speed/position of the hull. The estimated position information was corrected using GPS, and the estimated angle information was corrected using a magnetic compass. In addition, the accuracy of the estimated speed and position was further improved by correcting the speed using the encoder proposed in this study. Fig. 6 shows the platform used in the performance tests.

Fig. 6. Environment of navigation experiment.

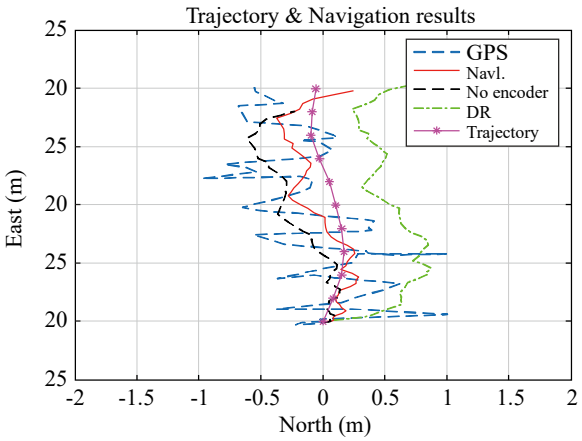

Fig. 7. Results of basic performance experiments.

1) Basic Navigation Performance Test

In the first experiment, the basic performance of the navigation system was verified. The platform position was measured after moving the underwater track robot straight 20 m in the east axis direction and the measured position and the results from the navigation system were compared. The position on the north axis was measured by marking every 2 m along the east axis and taking a photograph whenever the platform passed the marked position. In Fig. 7, GPS denotes the GPS measurement position (long dotted line), Navi. denotes the proposed navigation estimation position (solid line), No encoder denotes the navigation estimation position without speed correction by an encoder (short dotted line), DR system is the estimated position by DR (dot-solid line), and trajectory is the actual measured position (star solid line). Although the driving speed of both motors mounted on the underwater track robot was set to 2000 rpm for straight movement, the robot moved along a nearly curved line rather than a completely straight line because of the ground conditions and various environmental factors.

The experimental results in Fig. 7 show that the estimated position of the proposed navigation was similar to the actual

Table 4. Position error result of navigation experiments.

Index	Position Error		Units
	X	Y	
1	-0.0025	-0.0116	m
2	-0.0004	0.0231	
3	0.1299	0.0843	
4	-0.1078	0.1220	
5	0.1021	-0.1289	
6	0.0777	-0.2864	
7	0.2418	-0.2198	
8	0.0292	-0.1160	
9	0.1189	-0.2148	
10	0.2670	-0.1013	
11	-0.0138	0.5503	
RMS Error	0.13	0.22	

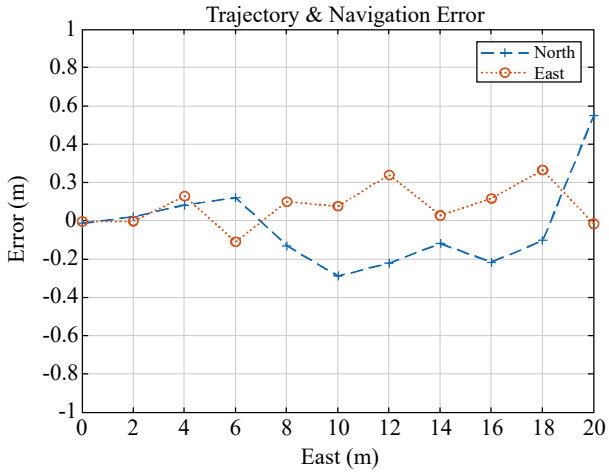

Fig. 8. Error between trajectory and navigation position results.

position, whereas the estimated position of the DR system was slightly different. The DR system estimated the position in a direction different from the moving direction of the platform from the initial estimation position, and it did not converge to the reference position value even at a later time. A DR system may have a larger error when the experimental time increases. Although the navigation without encoder information did not have a large error, as it also performs the position correction step through GPS similar to that of the proposed navigation method, the estimated position was slightly different. When looking at the position measured by GPS during the experiment, there was a somewhat large error due to the horizontal precision of the sensor itself. It was found that the proposed navigation position was very close to the actual measured position compared to the other navigation results.

Fig. 8 shows the error between the measured position and the proposed navigation position for each axis. The north axis

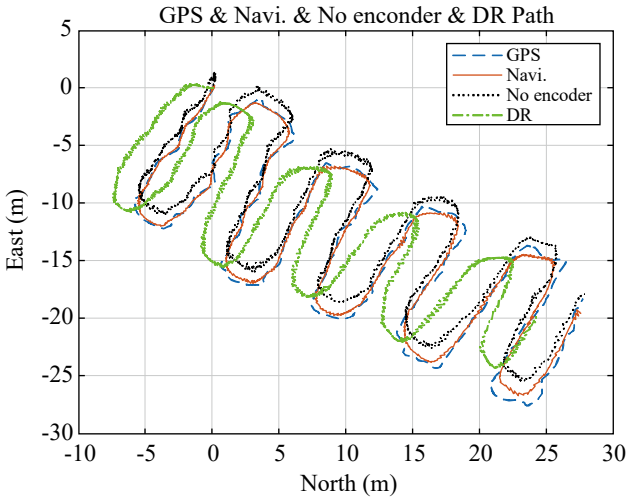

Fig. 9. Position results of each navigation.

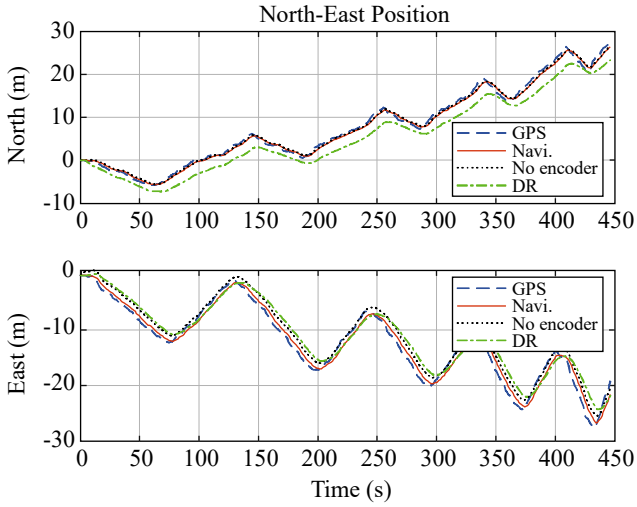

Fig. 10. North-east position results of each navigation.

is marked with +, and the east axis is marked with O. A total of eleven comparisons were performed and the results are shown in Table 4. The maximum error per axis was calculated as [0.267 0.5503] m and the RMS error was calculated as [0.13 0.22] m. From the experimental results, it was found that the proposed navigation method estimated the position within 0.3m of the RMS error.

2) Performance Test of the Zigzag Trajectory Navigation

In this experiment, the results of the proposed navigation, the results of the navigation without velocity correction by the encoder, and the results of the DR system were compared. The driving speeds of both motors mounted on the underwater track robot were set to 3000 rpm. As shown in Fig. 9, the robot started at the [0 0] m position, moved in a zigzag-shaped repeated trajectory, and stopped at the [27 -20] m position. The purpose of this experiment is to check the estimation capability of the navigation position error in an environment where the moving direction of the hull continuously changes to the left and right. In this experiment, it was difficult to measure the platform position; hence, the navigation results were compared to the reference value, that is, the position measured by GPS. In Fig. 9, GPS denotes the GPS measurement position (long dotted line), Navi. denotes the proposed navigation estimation position (solid line), No encoder denotes the navigation estimation position without speed correction by an encoder (short dotted line), and the DR system denotes the estimated position by DR (dot-solid line). The navigation duration was approximately 450 s between the start and stop of the underwater track robot.

The experimental results in Fig. 9 show that the estimated position of the proposed navigation and the estimated position of the navigation without encoder information were similar to the GPS measured position, whereas the estimated position of the DR system was slightly different. The DR system estimated the position in a direction different from the moving direction of the platform from the initial estimation position and it did not converge to the reference position value even at a later time. A DR system may have a larger error when the experiment time increases. Although the navigation without encoder information did not have a large error, as it also performed the position correction step through GPS similar to that of the proposed navigation method, the estimated position was slightly different.

Fig. 10 shows the comparison per axis for the results shown in Fig. 9. The estimated positions of the X and Y axes both show a zigzag shape; the X coordinate (north) continuously increases and the Y coordinate (east) continuously decreases. The error increased when the moving direction of the hull was changed and there was a repeated convergence over time. The position error is expressed as the difference between the estimated and reference position values of the proposed navigation method. The largest error was approximately 2 m on the X-axis, approximately 2.2 m on the Y-axis, and the position RMS error is calculated as [0.98 1.29] m.

Fig. 11 shows the velocity components estimated from the proposed navigation, navigation without encoder information, and DR system. If you check the speed result of the proposed navigation, the maximum speed for each axis was [0.46 0.7] m/s and the average speed was [-0.07 0.01] m/s. The Y-axis velocity of the navigation without encoder information was estimated to be slightly higher than that of the proposed navigation, and it had a larger noise component. In addition, the X-axis velocity of the DR system was estimated in the opposite direction from the beginning, and the estimation was slightly lower than the X-axis velocity of the proposed navigation throughout the entire experiment. In addition, the Y-axis velocity was estimated to be slightly higher than that of the proposed navigation method. These errors in the estimated velocity seemed to be a factor in increasing the error value of the estimated position which was the final result of DR system and the proposed navigation without encoder information.

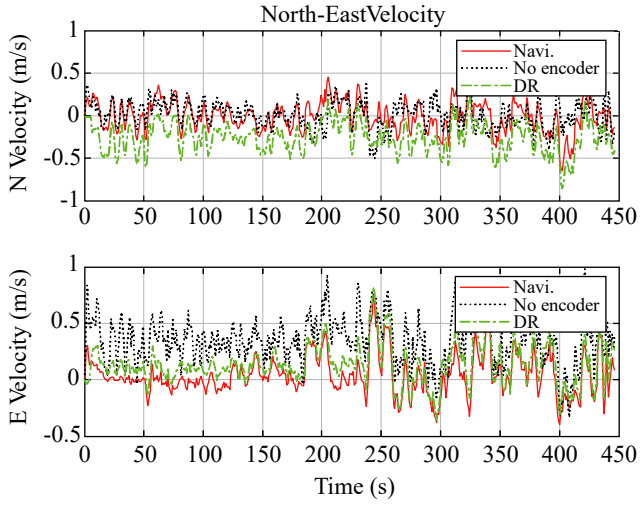

Fig. 11. North-east velocity results of each navigation.

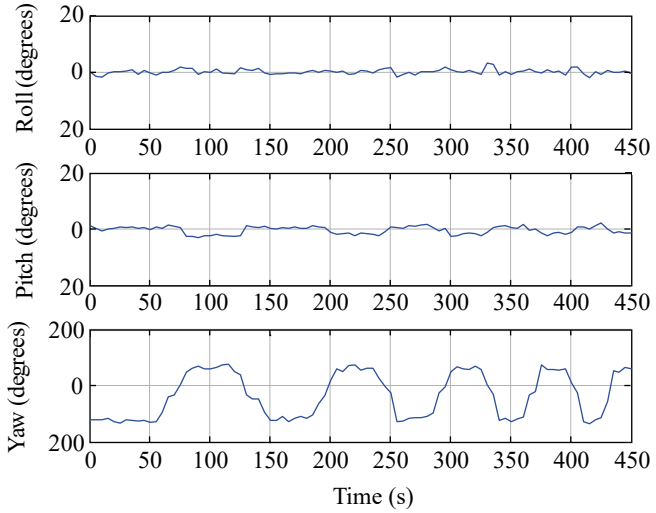

Fig. 12. Orientation results of navigation.

Fig. 12 shows the angle results of the proposed navigation system. The roll and pitch almost converged to 0 ° during the experiment and the angle of the traveling direction of the platform changed slightly when the platform rotated. In the case of heading, the hull's travel direction was changed nine times from -125 ° to 55 ° at approximately 180° intervals. Specifically, the platform made a U-turn at approximately 80, 120, 190, 240, 290, 340, 370, 410, and 430 s during the experiment

From the experimental results, the position data measured from GPS in real time had high noise; however, the results from the proposed navigation algorithm had much lower noise in the position data. In addition, when comparing the results of navigation without encoder information and DR to the proposed navigation, it was found that the provided navigation estimated a position more effectively and provided significant advantages.

V. CONCLUSION

Platforms operating on the seafloor, such as underwater track robots, cannot use a DVL, which is the most important sensor for underwater robots. To resolve this problem, this study investigated how to compensate for velocity by using the information of an encoder that can measure velocity instead of a DVL. First, we designed an integrated navigation algorithm. The INS was configured using an IMU, and the velocity from the INS was corrected with the encoder information of the track, which was corrected with GPS or USBL (horizontal), depth sensor (vertical), and the orientation angle was corrected with a magnetometer. Finally, the results (velocity, position, and direction angle) were calculated using an extended KF. Later, to verify the performance of the proposed integrated navigation algorithm, we developed an underwater track robot with an underwater navigation system. Finally, the integrated navigation performance was tested on land using the developed underwater navigation system and the fabricated underwater track robot. Although the system was experimented with on the ground, all the navigation sensors were the same as under the water, except for the USBL. However, GPS has the same role as the USBL such that GPS was used in the experiment. The experiments were performed on the ground because it is extremely difficult to accurately track the UTV underwater.

From the first experiment, it was found that the basic performance of the navigation system was within 0.3m of the position RMS error (compared to the actual position). In the second experiment, we compared the performance of the proposed navigation and other navigation methods. It was found that navigation without encoder information had some error and noise in the velocity component. It was also found that the initial velocity component of the DR system had a different direction, and the DR system had a relatively larger velocity error during the experiment. These errors in the estimated velocity seemed to be a factor that increased the error value of the estimated position which is the final result of the DR system and the proposed navigation without encoder information.

From the experimental results, when comparing the results of navigation without encoder information and DR to the proposed navigation, it was found that the proposed navigation was more effective in position estimation. The position data measured from USBL/GPS in real time had high noise; however, the results from the proposed navigation algorithm had much lower noise in the position data. In addition, when comparing the results of other navigation methods (DR system and without encoder information) to the proposed navigation, it was found that the proposed navigation showed a reduced error in position and thus estimated the position more accurately.

ACKNOWLEDGMENT

This research was supported by Unmanned Vehicles Core

Technology Research and Development Program through the National Research Foundation of Korea (NRF) and Unmanned Vehicle Advanced Research Center (UVARC) funded by the Ministry of Science and ICT, the Republic of Korea (NRF-2020M3C1C1A02086321), and "Data Collection System with Under Water Glider (19AR0001)" funded by Agency for Defense Development, Korea.

REFERENCES

Alahyari, A., S. G. Rozbahani, A. Habibzadeh, R. Alahyari and M. Dousti (2011). INS/DVL positioning system using Kalman filter. Aust. J. Basic Appl. Sci 5, 1123-1129.

Brunner, T., J. P. Lauffenburger, S. Changey and M. Basset (2015). Magnetometer-augmented IMU simulator: In-depth elaboration. Sensors 15(3), 5293-5310.

Hostettler, R. and S. Sarkka (2016). IMU and magnetometer modeling for smartphone-based PDR. In 2016 International Conference on Indoor Positioning and Indoor Navigation, 1-8.

Ji, D. H., H. S. Choi, S. K. Jeong, J. Y. Oh, S. K. Kim and S. S. You (2019a). A study on heading and attitude estimation of underwater track vehicle. Advances in Technology Innovation 4(2), 84-93.

Ji, D. H., H. S. Choi, M. T. Vu, N. D. Nguyen and S. K. Kim (2019b). Navigation and Control of Underwater Tracked Vehicle Using Ultrashort Baseline and Ring Laser Gyro Sensors. Sensors and Materials 31(5), 1575-1587.

Jeong, S. K., H. S. Choi, D. H. Ji, D. W. Jung, O. S. Kwon, C. J. Shin and J. M. Seo (2017). Study of ARS using Ring Laser Gyro. Journal of Ocean Engineering and Technology 31(2), 164-169.

Jung, D. W., S. M. Hong, J. H. Lee, H. J. Cho, H. S. Choi and M. T. Vu (2018). A Study on Unmanned Surface Vehicle Combined with Remotely Operated Vehicle System. Proceedings of Engineering and Technology Innovation 9, 17-24.

Karamat, T., M. Atia and A. Noureldin (2015). An enhanced error model for EKF-based tightly-coupled integration of GPS and land vehicle's motion sensors. Sensors 15(9), 24269-24296.

Lee, P. M., B. H. Jeon, S. M. Kim, H. T. Choi, C. M. Lee, T. Aoki and T. Hyakudome (2004). An integrated navigation system for autonomous underwater vehicles with two range sonars, inertial sensors and Doppler velocity log. MTTS/IEEE TECHNO-OCEAN'04 3, 1586-1593.

Lee, P. M., B. H. Jun, K. Kim, J. Lee, T. Aoki and T. Hyakudome (2007). Simulation of an inertial acoustic navigation system with range aiding for an autonomous underwater vehicle. IEEE Journal of Oceanic Engineering 32(2), 327-345.

Lee, P. M., H. W. Shim, H. Baek, B. H. Kim, J. Y. Park, B. H. Jun and S. Y. Yoo (2017). Navigation System for a Deep-sea ROV Fusing USBL, DVL, and Heading Measurements. Journal of Ocean Engineering and Technology 31(4), 315-323.

MathWorks, 2018. Sensor Fusion and Tracking Toolbox:Reference. MathWorks Inc, Massachusetts.

Munguía, R. (2014). A GPS-aided inertial navigation system in direct configuration. Journal of applied research and technology 12(4), 803-814.

Park, J. G. (2014). Vehicle Navigation System Design and Implementation using Integrated GNSS/INS/Odometer/Barometer Navigation System. M. S. Thesis, Chungbuk National University, Chungbuk, Republic of Korea.

Penas, A. A. (2009). Positioning and navigation systems for robotic underwater vehicles. Ph.D. Thesis, Instituto Superior Tecnico, Lisbon, Portugal.

Qi, H. and J. B. Moore (2002). Direct Kalman filtering approach for GPS/INS integration. IEEE Transactions on Aero-space and Electronic Systems 38(2), 687-693.

Ridao, P., D. Ribas, E. Hernandez and A. Rusu (2011). USBL/DVL navigation through delayed position fixes. In 2011 IEEE International Conference on Robotics and Automation, 2344-2349.

Ribas, D., P. Ridao, A. Mallios and N. Palomeras (2012). Delayed state information filter for USBL-aided AUV navigation. In 2012 IEEE International Conference on Robotics and Automation, 4898-4903.

Siouris, G. M. (2004). Missile guidance and control systems. Springer Science & Business Media, New York.

Somers, W. (2011). Doppler-based localization for mobile autonomous underwater vehicles. M.S. Thesis, Rutgers University, New Jersey, USA.

Sukkarieh, S., E. M. Nebot and H. F. Durrant-Whyte (1998). Achieving integrity in an INS/GPS navigation loop for autonomous land vehicle applications. Proceeding of 1998 IEEE International Conference on Robotics and Automation (Cat. No. 98CH36146) 4, 3437-3442.

Titterton, D. and j. Weston (2004). Strapdown inertial navigation technology. 2nd Ed. The Institution of Engineering and Technology, London.

Yunchun, Y. and J. A. Farrell (2003). Magnetometer and differential carrier phase GPS-aided INS for advanced vehicle control. IEEE Transactions on Robotics and Automation 19(2), 269-282.